International Journal of Nanoelectronics and Materials

In Press, Accepted Manuscript – Note to user

Synthesis and characterizations of structural, dielectric and optical properties of CCTO – PT composite.

N. Gouitaa[1,*], N Hadi[1,2], T Lamcharfi[1] and F Abdi[1]

[1] Laboratory of Signals, Systems and Components, University of Sidi Mohamed Ben Abdellah, USMBA. FST Fez, B.P. 2202, Morocco.

[2] Laboratory of Science faculty, university of Aden, Yemen, PO Box 6312, Aden, Aden, Yemen.

Received 11 April 2022, Revised 13 August 2022, Accepted 12 September 2022

ABSTRACT

In this study, we have synthesized the (1-x) $CaCu_3Ti_4O_{12}$ – (x) $PbTiO_3$ (CCTO-PT) composites with x = 0.00, 0.50 and 1.00 by using the solid-state method. We have then studied the structural, optical and dielectric properties of these composites. The X-ray diffraction diffractogram (XRD) showed that the ceramics at x = 0.00 and 1.00 (CCTO and PT) crystalize in a pure cubic and tetragonal phase respectively. Likewise, for CCTO-PT composite, we observed a coexistence of tetragonal and cubic phase in CCTO-PT composite composites. The scanning electron microscopy (SEM) micrographs showed homogeneous microstructure samples and consist of different grain shape. The large spherical grain structure is attributed to CCTO ceramic while the smaller grain form can be ascribed to the PT ceramic. The dielectric measurements results revealed an increase in dielectric permittivity value for CCTO-PT composite compared with pure CCTO and PT. The optical band gaps of the CCTO and PT are 2.50 and 3.00 eV, and increased to 3.50 eV for the CCTO/PT composite.

Keywords: Dielectric measurements, optical, permittivity, SEM, X-ray diffraction.

1. Introduction

Nowadays, many attentions have been paid to cubic perovskite $CaCu_3Ti_4O_{12}$ (CCTO) due to it important dielectric properties which make it very useful in microelectronic devices [1-6]. However, CCTO ceramic exhibits a high dielectric permittivity (in order to 10^4) at room temperature and it remain almost constant at a large temperature range between 100 K and 600 K. There is no structural phase transition found in CCTO ceramic in this range of temperature, which make it desirable for practical electronic devices [7,8]. On the other hand, lead titanate $PbTiO_3$ (PT) based ceramic is considered as one of the most used ferroelectric materials in transducers, actuators, sensors and capacitors devices [9-11]. It is the simplest perovskite, that presents stable dielectric properties in a large range of temperature and frequencies, and possess a high dielectric transition (490 °C) [12,13]. This high phase transition temperature is requested for ferroelectric materials. The PT has a high tetragonal distortion (c/a~1.064) [14] which makes it significantly more ferroelectric with highest spontaneous polarization [15-16]. But, $PbTiO_3$ is not environmentally safety material because the Pb has a high toxic in nature, this is why there is a necessity to reduce Pb content in applications from safety and health concerns. So, one of the approaches is to synthesis it with a composite material.

However, all the researchers reported that the CCTO system has a cubic structure [17], supported by it non ferroelectric behavior that further confirmed by the structural analysis. To make this material ferroelectric, we thought about compounding it with PT ferroelectric material. Also, to improve the dielectric permittivity, we have chosen the PT material. From these points of view, the (1-x) CCTO-xPT solid solutions can be very useful. Lili Zhao et al [18] reported the giant dielectric phenomenon of BST-CCTO multilayers which is far more than the dielectric permittivity

of CCTO or BST ceramics alone. Other researchers reported a significantly improvement of giant dielectric properties of $CaCu_3Ti_4O_{12}$ ceramics with another approach which consists by co-substituting this material with other ions such as Sr^{2+} and F^- ions [19] and substitution it with either Al^{3+} or Ta^{5+} ions [20].

There is a similar work that we have studied which is focused in structural and dielectric properties of CCTO-PT for x=0.0 to 1.0, that is published recently [21]. The result found confirm that the PT increases the dielectric permittivity of CCTO ceramic for all the PT content. But we noticed that the PT decreases the diffused character between x = 0.4 and 0.6So, we have chosen the x = 0.5 rate of PT, to confirm the evolution of these dielectric properties. There are similar works we carried out in (1-x)CCTO-xPZT [22], (1-x)CCTO-x$BaTiO_3$ [23] and BST-CCTO [18]. In this work, we have investigated the effect of adding PT on structural properties of CCTO ceramic at x=0.5. The microstructure properties of the powders have been investigated using X-ray diffraction (XRD) patterns and scanning electron microscopy (SEM). The temperature and frequency variation of the dielectric properties has also been investigated. Finally, the optical results were discussed.

2. Experimental methods

The (1-x)CCTO-xPT (where x = 0.00, 0.50 and 1.00) ceramic composites were prepared by combining the solid state and sol-gel reactions. In the beginning, we prepare the CCTO by a solid-state reaction using $CaCO_3$ (purity 99.5 %), CuO (purity 99.7 %) and TiO_2 (purity 99.8 %), as raw materials. These materials were weighted in stochiometric proportion and were blended using an agate mortar for 1h, after that milled with the acetone for 3h. The obtained powder was calcined in air at 1050 ^{0}C for 4h.

After that the PT ceramic powder was prepared by a sol-gel method. The starting materials were the lead (II) acetate trihydrate ($Pb(CH_3COO)_2.3H_2O$, purity 99%) and titanium isopropoxide, ($Ti(OCH(CH_3)_2)_4$, 97%). The titanium isopropoxide was mixed with the lactic acid and water. The resulting dispersion was heated on a hot plate under stirring at 70–80 °C to get a homogenous sol (titanium sol). Afer which, the lead acetate was dissolved in distilled water and mixed with titanium sol and placed in the oven for 48 h then the dry gel was calcined at 700 °C for 4 h in the atmosphere.

In the final step, the (1-x) CCTO-xPT composites were synthesised by using the calcined CCTO and PT and they were mixed in stochiometric proportion using an agate mortar for 1h, then milled under acetone for 2h. The obtained powder was dried at 400 °C for 2h.

To study the structural properties of these powders, we have used the X-Ray Diffraction (XRD) and the Rietveld refinement. These analyses are performed using a Siemens X'Pert diffractometer. The monochromatic X–ray radiation is produced by a copper anticathode Kα line. The spectra are recorded at the speed 0.02°/min. The filter is a nickel pellet (Ni) for filtering the doublet $K\alpha_1$, $K\alpha_2$ characterized by an average wavelength λkα = 1.5406 Å. The continuous acceleration voltage used is 40 kV and the heating current is 30 mA. A computer that gives access to all these functions controls the system. The obtained results were fitted using the Rietveld method in fullProf software. The UV–visible scattering spectra of the samples are recorded using the JASCO V–570 spectrometer (LASMAR Laboratory, FSM–Meknes).

The pellets were also prepared for scanning electron microscope (SEM) and dielectric measurements. So, these powders were mixed with adding the polyvinyl alcohol (PVA) as a binder, and pressed using an uni-axial press to form a pellet, with diameter of 12 mm and thickness of 1mm, which were sintered at 1000°C/8h. The sintered samples were characterized by SEM and a metal layer was deposited on both sides of the pellet for electrical and dielectric properties measurements. In this work, we coated both sides of the pellets, with silver paste in thin layer. The pellets are heated at 150 °C for 30 min to ensure the silver paste deposition on the pellet's sides.

3. Results and discussion

3.1. Structural properties of (1–x) CCTO–x PT: XRD results

The XRD patterns recorded for CCTO (calcined at 1050 ^{0}C/4h), PT (calcined at 700 ^{0}C/4h) and CCTO–PT samples at room temperature are shown in figure1.(a). The diffraction pattern consists of well–resolved peaks which have been indexed to Im–3 and P4mm space group for the both pure CCTO and PT with cubic and tetragonal symmetry, respectively. For the CCTO–PT composite, all the observed peaks indexed to Im–3 and P4mm space groups.

To confirm this, the XRD pattern of CCTO, PT and CCTO–PT have been fitted using the Rietveld method in Fullprof Suite program [23] and the results are shown in figure. 1 (b)-(d). In these figures, the experimental curves are given as black line and theoretical data are shown as the red lines. The difference between theoretical and experimental data is shown as the bottom line (green). The vertical lines represent the Bragg's allowed peaks. The XRD peaks are fitted by using Im–3 and P4mm space groups corresponding to cubic and tetragonal symmetry for CCTO and PT, respectively. The difference between experimental and refined data is found to be minimal for CCTO-PT composite which confirm a better crystallinity of this powder.

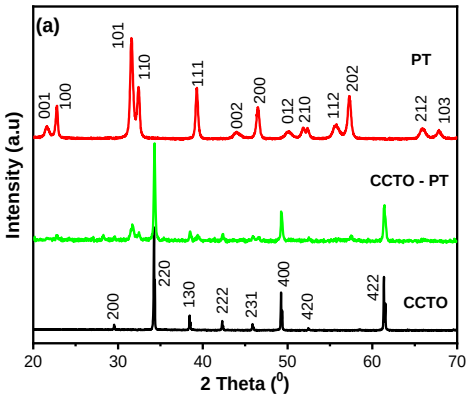

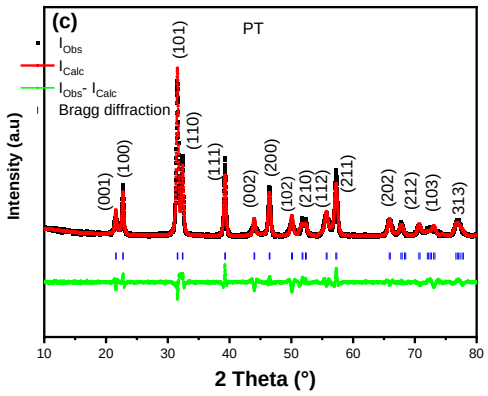

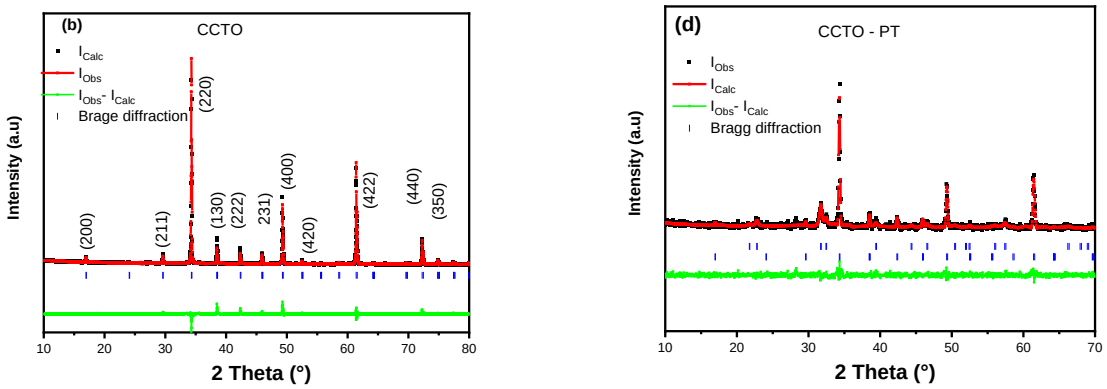

Figure. 1 (a). The XRD pattern of CCTO, Pt and CCTO-PT samples. Rietveld refinement for **(b)** pure PT **(c)** pure CCTO and **(d)** CCTO-PT composites.

The Reliability factors, R_{Bragg}, R_F and χ^2 found from fitting are shown in Table.1. We observed a low value of X^2 of all the powders which confirm a good refinement of the powders. The Rietveld refinement lattice parameters and unit cell volume are also shown in Table 1. From Rietveld analysis the unit cell parameters values are of a=b= c=7.391 Å for pure CCTO which are in good agreement with those reported in literature [24, 25]. While, the lattice constants of $PbTiO_3$ are a=b= 3.909 Å and c = 4.116 Å with axial ratio c/a is found 1.052. The axial ratio found in this study is less than the reported value of 1.0614 [26] which indicate that our material is more compact and the structure is more stable.

Table 1. R-factors, lattice parameters, and volume of the CCTO, PT and CCTO-PT samples.

Parameters	Values CCTO pure	Values PT pure	Values CCTO in mix.	Values PT in mix.
R_{Bragg}	10.7	3.95	4.58	8.56
R_F	13.9	2.33	5.22	6.61
X^2	1.21	2.43	1.14	1.14
D (Å)	949.540	147.635	539.23	102.25
lattice constants (Å)	a=7.391	a=b= 3.909 c= 4.113, c/a= 1.052	a=b =c=7.390	a=b=3.900, c=4.086, c/a =1.048
V (Å^3)	403.665	62.839	403.816	62.133

The fractional atomic positions of the atoms in PT and CCTO unit cell in the pure and in the mixture obtained from Rietveld refinement are given in Table 2 and Table 3. for the position of the Pb, Ti and O atoms in PT unit cell (Table.3), we refined two oxygen positions. The occupancy is considered as fixed because the atom is lighter, so it is not very sensitive to the XRD and it is difficult to refine this oxygen occupancy from XRD data. It is observed from Table 2 that the positions of Pb, Ti and O are affected by mixing with CCTO. This effect is clearly observed in the atomic positions of the z-axis. Meanwhile, the positions of Ca, Cu, Ti, and O in CCTO unit cell (Table 3) did not change. These values are found to be of the order of those reported in the literature for PT [24-26] and for CCTO [27].

Table 2. Position parameters of Pb, Ti, O1 and O2 in PT unit cell for pure and mixture form.

Atom	Pure PT			PT in mixture		
Coordinate	X	Y	Z	X	Y	Z
Pb	0.012	0.012	9.700	0.023	0.023	9.772
Ti	0.500	0.500	10.153	0.500	0.500	10.264
O1	0.500	0.500	9.851	0.500	0.500	9.942
O2	0.500	0.000	9.273	0.500	0.000	9.446

Table 3. Position parameters of Ca, Cu, Ti and O in CCTO unit cell *for pure and mixture form.*

Atom	Pure CCTO			CCTO in mixture		
Coordinate	X	Y	Z	X	Y	Z
Ca	0.000	0.000	0.000	0.000	0.000	0.000
Cu	0.000	0.500	0.500	0.000	0.500	0.500
Ti	0.250	0.250	0.250	0.250	0.250	0.250
O	0.310	0.180	0.000	0.298	0.187	0.000

Bond lengths are generated for the refined structures of PT and CCTO before and after mixing them up, the bond lengths are calculated with VESTA program, the results are listed in Table 4 for PT as an example. The fitting profile data indicate a slight change in Pb-O1 liaison value from PT to the PT in mixture form compared with Pb-O2 bond where the change is more important. While for Ti–O1 and Ti–O2 liaison, we can notice a slight value variation from pure PT to the PT in the mixture (table4). On the other hand, for the CCTO, each metal–oxygen bond length is calculated in the pure CCTO phase and in CCTO in the mixture form. Regarding the values reported in table.5, we notice a slight variation in all the Oxygen-metal (Ti, Ca, or Cu) length.

Table 4. Calculation of the length of the Pb –O, Pb –O2, Ti–O1 and Ti–O2 bonds in the PT structure obtained from Rietveld analysis obtained from Rietveld analysis.

Parameters	Pure PT	PT in mixture
Pb –O1	2.833	2.844
Pb –O2	2.627	2.362
Ti–O1	1.243	1.3174
Ti–O2	2.015	2.086

Table 5. Calculation of the length of the metal–oxygen bond in the CCTO structure obtained from Rietveld analysis.

Parameters	Pure CCTO	CCTO in mixture
Ca – O	2.601	2.601
Cu –O	1.996	2.033
Ti–O	1.957	1.938

The structure of the compounds is shown in figure 2. This structure has been drawn using the refined parameters.

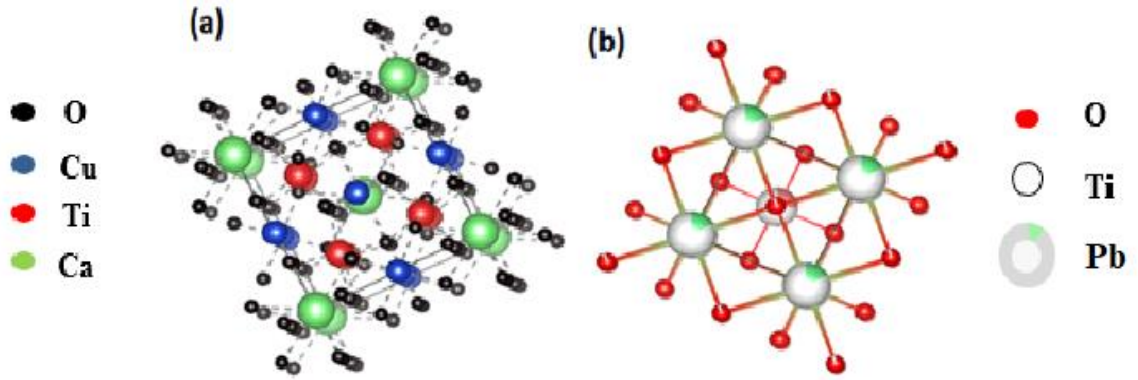

Figure 2. Structure of $CaCu_3Ti_4O_{12}$ and $PbTiO_3$ obtained from the Rietveld analysis parameters.

3.2. Microstructural properties of (1–x) CCTO–x PT: SEM results

The surface morphology of CCTO, PT, and CCTO–PT samples sintered at 1000 ^{0}C/8 h is shown in Fig. 3. It can be seen in the the figure 3. (a), that the shape and distribution of grains in the microstructure confirm the polycrystalline nature of the samples. The microstructure of the pure CCTO ceramic is characterized by well-developed and a large spherical grain structure separated from each other by clear borders, and consisting also of grains with smooth surfaces. The microstructure of pure PT ceramic (Figure 3 (b)) is not similar to the microstructure of the CCTO ceramics. However, there are a significantly smaller grains and more condenser surfaces compared with CCTO ceramic. In the case of mixture ceramic of CCTO and PT (Figure 3 (c)), the microstructure of pellet is similar to the pure PT and consists of much smaller well–crystallized grains with less pores number compared to the PT pellet always with presence of condenser surfaces. Some small particles and deposits are observed between grains, which is related to the partial CCTO decomposition and segregation of oxides during the sintering at high temperature [29]. The grain size of CCTO, PT, and CCTO–PT is in the range of 2–17 µm, 0.2–3.0 µm and 0.1–2 µm, respectively. So, the PT addition reduce the grain size of CCTO–PT.

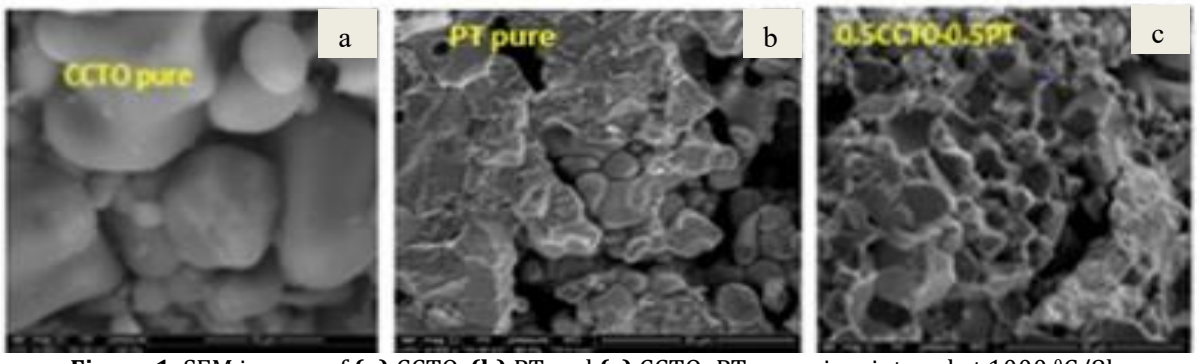

Figure 1. SEM images of **(a)** CCTO, **(b)** PT and **(c)** CCTO–PT ceramics sintered at 1000 ^{0}C/8h.

3.3. Dielectric properties of (1–x) CCTO–x PT

The temperature dependence (R.T to 450 ^{0}C, according to the possibility of the laboratory) of dielectric permittivity at different frequencies of the pure CCTO, pure PT, and CCTO–PT

composites pellets sintered at 1000 ^{0}C/8 h is shown in Figure 4. For the pure PT sample synthesized by sol–gel route, the dielectric constant shows a slight increase with temperature up to 300 ^{0}C, then a rapid increased to a maximum value at 450 ^{0}C and there is no evidence of transition temperature within the measurement range (Fig.4 (a)). This result is expected because the pure PT has a phase transition temperature from ferroelectric to paraelectric at 490 ^{0}C [12,24]. Whereas, for pure CCTO ceramic (Fig.4 (b)), a broad dielectric plateau (peak–like) appears near 200 ^{0}C, which shifts to higher temperatures with increasing frequency. Such a behavior is similar to the ferroelectric relaxer in the ceramic materials. We can also observed a high diffuse character and the permittivity is almost stable at this range of temperature. In addition, another peak appears near 400 ^{0}C and suggests a relaxor phenomenon. In case of merging the two materials (0.50CCTO–0.50PT) pellet, the dielectric constant shows a widely dielectric anomaly with shifts toward right compared to CCTO (Fig. 4 (c) and Fig.4 (d)). However, CCTO–PT peaks indicate a frequency dispersion due to no normal ferroelectric behavior (Figure 4 (c)) suggesting that CCT'O behavior dominates the PT behavior.

As it is observed in Figure 4 (d), the CCTO–PT dielectric permittivity has highest value at all temperature and frequencies ranges compared with pure samples. This increase is may be related to the layer (layer has different electrical properties) formation in the area near the phases explained in terms of an internal barrier layer capacitor (IBLC) structure of thin insulating grain boundaries (GBs) and conducting grain interior (bulk) regions [30, 31]. The origin of the IBLC structure is due to a small Cu non-stoichiometry introduced in CCTO structure, which take place between the GBs and bulk. On the other hand, the value of dielectric permittivity of CCTO-PT is three time more than that of pure CCTO due to the condenser surfaces observed in SEM results for CCTO-PT ceramic. This increase in permittivity is also observed in our previous work on the same CCTO-PT composites (for x=10 to 100%) [21] and also in the literature for BST-CCTO composite [18].

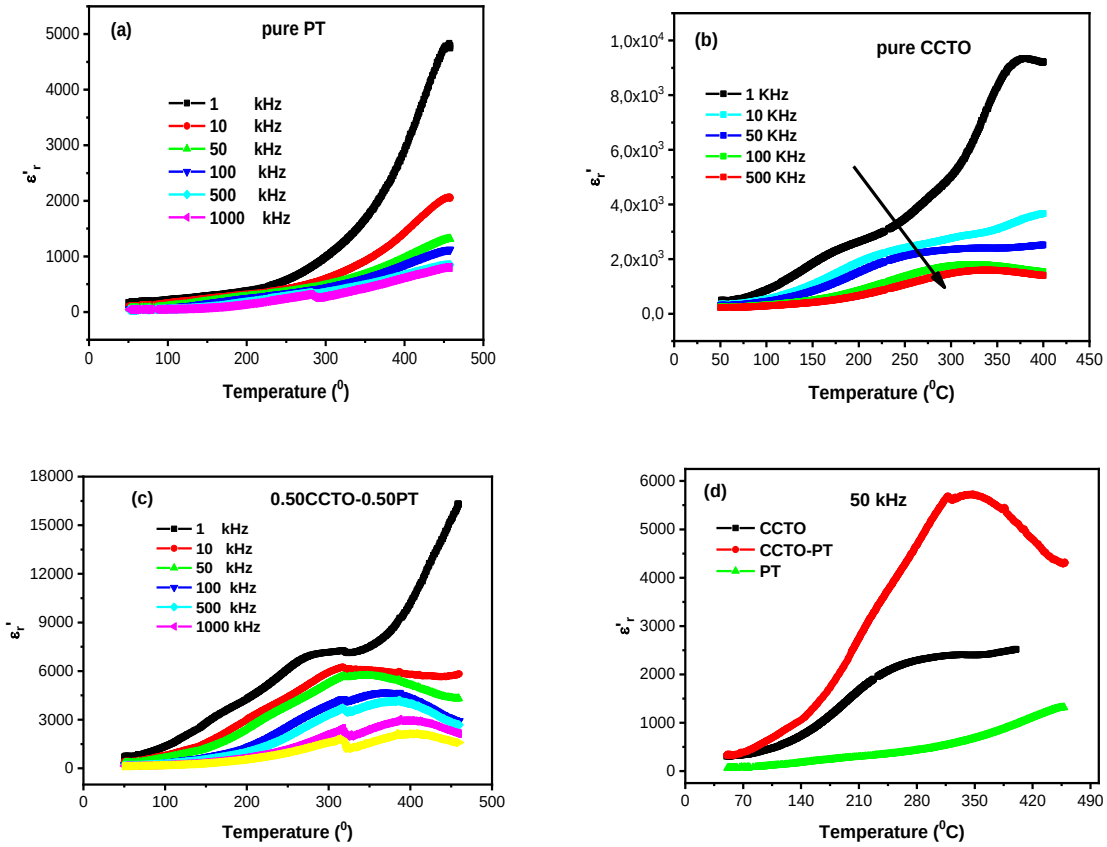

Figure 4. Temperature dependence of dielectric constant of the ceramics sintered at 1000 ^{0}C/8h for; **(a)** pure PT at different frequencies, **(b)** pure CCTO at different frequencies, **(c)** CCTO-PT composite at different frequencies and **(d)** CCTO, PT and CCTO-PT at 50 kHz.

Figure 5 showed the evolution of dielectric permittivity and losses as function of frequency for all the PT, CCTO and CCTO-PT samples. We can notice a clear decrease of dielectric permittivity with increasing frequency at low frequency region. While at high frequency region the permittivity remains constant with the frequency variation which confirm the ferroelectric behaviour evolution for these ceramics. Through, the evolution of dielectric loss for CCTO and CCTO-PT ceramics has the same evolution and follows the same evolution than the dielectric permittivity as function of frequency. While for PT ceramic, we observed an appearance of a maximum of dielectric losses at 10^5 of frequency.

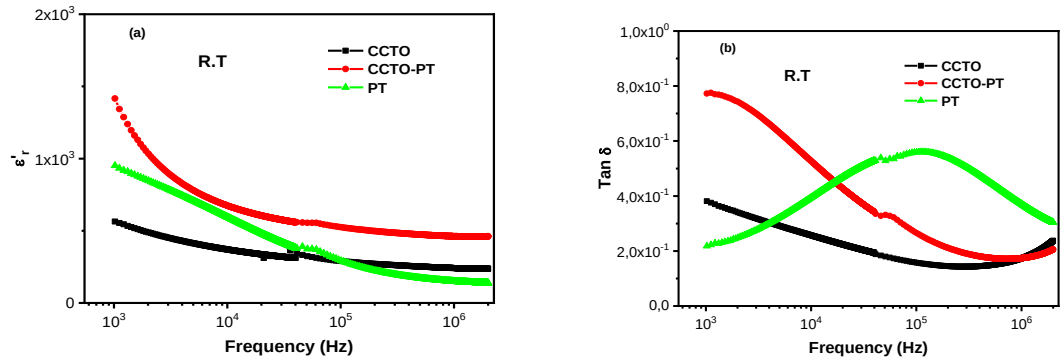

.

Figure 5. Dielectric constant and tan δ of CCTO, PT and CCTO–PT as function in frequency at R.T.

3.4. Optical properties

The UV–visible reflectance spectra of CCTO-PT perovskite materials are placed in barium sulfate plate ($BaSO_4$) as a standard (100 % reflectance) and analysed using Jasco V–570 spectrophotometer in the wavelength range [200–2000 nm] at room temperature. The Figure 6 shows the transmission spectra of different compounds. The analysis of spectra in the UV–vis domain shows that the percentages of transmission (T %, Figure 6) is greater than 99 % and 46 % in pure PT and CCTO respectively, which shows that pure PT compound has a very important optical transparency. In the other hand, the CCTO–PT showed the percentage of transmission which is about 76 % (Table 6).

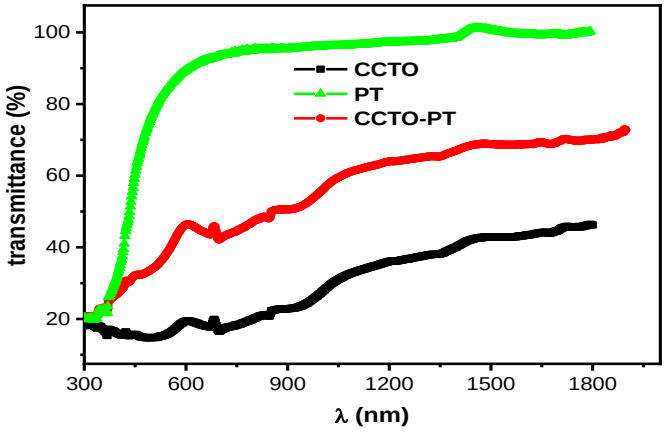

Figure 6. Optical Transmittance spectrum of CCTO, PT and CCTO–PT.

The band gap of the CCTO, PT, and CCTO–PT has been calculated from the transmittance edge of the spectrum by calculating the transmittance T (%) which is related to the optical absorption coefficient and the photon energy by the following expression.

$$\alpha = \frac{ln^{1}/_{T}}{d} \quad (1)$$

where d is the thickness of the pellet (0.76 mm). So, the energy band gap (E_g) can be estimated by assuming direct transition between conduction band and valance band using the following expression:

$$\alpha = A(hv - E_g)^{1/2} \quad (2)$$

where A is the constant, E_g is the optical energy band gap, υ is the frequency of incident beam and h is Planck's constant. The direct band gap is determined using equation (2) when linear portion of $(\alpha hv)^2$ against hv plot is extrapolated to intersect the energy axis at α =0 (Figure 7 and Table 6). The values of energy band gap of the CCTO, PT and CCTO–PT composites-obtained are 2.50, 3. 00 and 3.50 eV, respectively. These values are in agreement with the review data reported previously [28] for CCTO and [32] for PT.

Table 6. Variation of transmittance and energy band gap (E_g) for (1–x) CCTO–xPT ceramics.

(1–x) CCTO–xPT	Trans. %	Eg (*eV*) In this work	Eg (*eV*) Refr.
x= 0.00	46.43	2.50	2.48 [21]
x= 0.50	76.24	3.50	

x= 1.00	99.85	3.00	3.45[22]

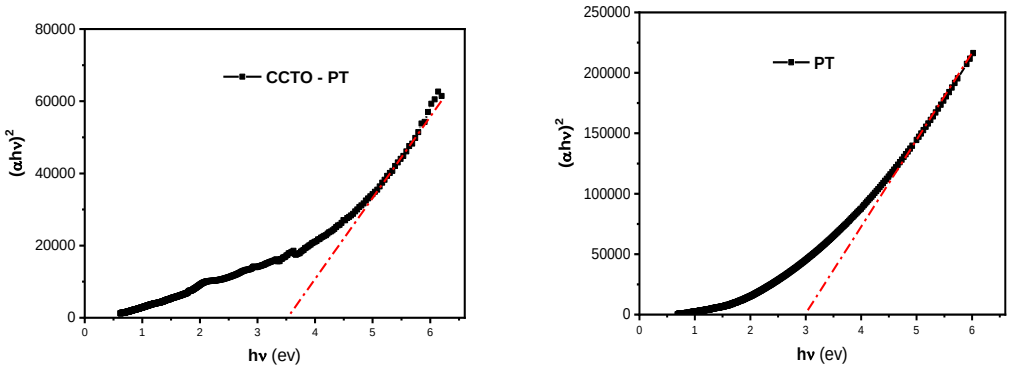

Figure 7. The optical band gap energy of CCTO–PT and PT.

4. Conclusion

In the present work, we have prepared CCTO– PT composite from CCTO and PT ceramics which were synthesized by solid state route and by sol gel route respectively. X– Ray diffraction pattern showed pure phase formation for both CCTO (cubic) and PT (tetragonal) and co–existence of cubic and tetragonal phases for CCTO– PT composite. From Rietveld analysis, we found that the unit cell parameters of CCTO and PT in the mixture decreased, as well as decrease in the axial ratio (c/a) of PT. A study of CCTO- PT dielectric properties showed an increase in dielectric permittivity value and ferroelectric relaxer behavior. The optical analysis of the samples indicated excellent optical properties, specifically light transmittance, which is estimated 99.85 % for pure PT and 76.24 for CCTO–PT composites. The values of the band gap energy are also found to be within the semiconductor ranges of all studies samples.

REFERENCES

[1]. Homes, C.C, Vogt,T., Shapiro, S.M., Wakimoto, S., and Ramirez, A.P, Science 293 (2001) 673 .

[2]. Subramanian, M.A, Dong, L., Duan, N., Reisner, B.A, and Sleight, A.W, J. Solid State Chem. 151 (2000) 323

[3]. Ramirez, A. P., Subramanian, M. A., Gardel, M., Blumberg, G., Li, D., Vogt, T., and Shapiro, S. M., Solid State Commun. 115 (2000) 217.

[4]. Subramanian, M. A., and Sleight, A. W., Solid State Sci. 4 (2002) 347.

[5]. Kim, Y. J., Wakimoto, S., Shapiro, S. M., Gehring, P. M., and Ramirez, A. P., Solid State Commun. 121 (2002) 625.

[6]. Adams, T. B., Sinclair, D. C., and West, A. R., Adv. Mater. ~Weinheim, Ger. 14 (2002) 1321.

[7]. Subramanian, M.A., Li, D., Duan, N., Reisner, B.A., Sleight, A.W., J. Solid State Chem. 151

(2000) 323–325.

[8]. Ramirez, A.P., Subramanian, M.A., Gardel, M., Blumberg, G., Li, D., Vogt, T., Solid State Commun. 115 (2000) 217–220.

[9]. Zhang, S. , Li, F. , Jiang, X., Kim, J., Luo, J., Geng, X., a review. Prog. Mater. Sci., 68 (2015) 66.

[10]. Lanki, M., Nourmohammadi, A., Feiz, S.M.H., Adarmanabadi, E.R, J. Ceram. Process. Res., 17 (2016) 394-400 .

[11]. Shrout, T. R., and Halliyal, A., American Ceramic Society Bulletin, 66 (1987)704–711.

[12]. Chan, Y., Chan, H. L. W., and Choy, C. L., Journal of the American Ceramic Society, 81 (1998) 1231.

[13]. Ting, R. Y., Ferroelectrics, 67 (1978) 143–157.

[14]. Zhao, H., Miao, J., Zhang, L., Rong, Y., Chen, J., Deng, J., Yu, R., Cao, J., Wang, H. and Xing, X., Dalton Trans.,45 (2016) 1554-1559.

[15]. Choudhary, R.N.P., and Mal, J., Mater. Sci. Eng., B, 2002, 90, 1-6. 17. D.I. Woodward and I.M. Reaney, Acta Cryst., B61 (2005) 387-399.

[16]. Irvine, J T S., Sinclair, D C., and West, A R., Advanced Materials, 2 (1990) 132-138.

[17]. Lin, H., Xu, W., Zhang, H., Chen, C., Zhou, Y, and Yi, Z., Journal of the European Ceramic Society, 40 (2020) 1957-1966.

[18]. Zhao,.L, Xu,.R, Wei, Y., Han, X., Zhai, C., Zhang, Z., Qi, X., Cui, B., Jones, J.L., Journal of the European Ceramic Society, 39 (2019) 1116-1121,

[19]. Jumpatam, J., Putasaeng, B., Chanlek, N. Boonlakhorn, J., Thongbai, P., Phromviyo, N., and Chindaprasirt, P., Materials Research Bulletin 133 (2020) 111043.

[20]. Boonlakhorn, J. , Chanlek, N., Manyam, J. , Srepusharawoot, P., Krongsuk, S. , Thongbai, P., Journal of Advanced Ceramics, 10 (2021) 0–0.

[21]. Slaoui, M., Gouitaa, N., Lahrichi, A., Harrach, A., , Haddad, M., and Lamcharfi, T., Asian Journal of Chemistry, 33 (2021) 1208-1214.

[22]. Hadi, N., Abdi, F., Lamcharfi T., Belaaraj, A., Kassou, S., and Ahjyaje, F.Z, Mediterranean Journal of Chemistry, 8 (2019) 245-254.

[23]. Young, R. A., International Union of Crystallography, New York, Oxford University Press (1996).

[24]. Cole, S.S., Espenschied, H., Journal of Physical Chemistry, 41 (1937) 445–451.

[25]. Jangade, P., Arjunwadkar, P. R., Nagarbawadic, M. A., Journal of Applied Physics, 8 (2016)

2278–4861.

[26]. Chaudhari, V.A., Bichile, G.K., Smart Materials Research, 2013 (2013) Article ID 147524, 9 pages.

[27]. Subramanian, M.A,, and Sleight, A.W., Sciences, 4 (2002) 347–351.

[28]. Mouraa, F., Cabral, A.C., Rochab, L.S.R., Aguiarc, E.C., Simõesb, A.Z., and Longoc, E., Ceramics International 42 (2016) 4837–4844.

[29]. Zhao, J., Liu, J., Ma, G., Ceramics International 38 (2012) 1221–1225.

[30]. Sinclair, D. C., Adams, T. B., Morrison, F. D., West, A. R., Appl. Phys. Lett. 80 (2002) 2153.

[31]. Adams, T. B., Sinclair, D. C., West, A. R., Phys. Rev. B , 73 (2006) 094124.

[32]. Thacher, P. D., Appl. Optics. 16 (1977) 3210.